Lung Cancer 132 (2019) 28–35

Contents lists available at ScienceDirect

Lung Cancer

journal homepage: www.elsevier.com/locate/lungcan

Radiomics signature: A potential and incremental predictor for EGFR mutation status in NSCLC patients, comparison with CT morphology

Wenting Tu[a,1], Guangyuan Sun[b,1], Li Fan[a,*], Yun Wang[a], Yi Xia[a], Yu Guan[a], Qiong Li[a], Di Zhang[a], Shiyuan Liu[a], Zhaobin Li[c,*]

[a] Department of Radiology, Changzheng Hospital, Second Military Medical University, No. 415 Fengyang Road, Shanghai 200003, China
[b] Department of Thoracic and Cardiovascular Surgery, Changzheng Hospital, Second Military Medical University, No. 415 Fengyang Road, Shanghai 200003, China
[c] Department of Radiation Oncology, Shanghai Jiao Tong University Affiliated Sixth People's Hospital, No. 600 Yishan Road, Shanghai 200233, China

ARTICLE INFO

Keywords:
Lung neoplasms
Radiomics
Tomography
X-ray computed
Epidermal growth factor receptor
Gene mutation

ABSTRACT

Objectives: To compare the predictive performance of radiomics signature and CT morphological features for epidermal growth factor receptor (EGFR) mutation status; then further to develop and compare the different predictive models for EGFR mutation in non-small cell lung cancer (NSCLC) patients.

Materials and methods: This retrospective study involved 404 patients with NSCLC (243 cases in the training cohort and 161 cases in the validation cohort). Radiomics features were extracted from preoperative non-contrast CT images of the entire tumor. Correlations between the EGFR mutation status and candidate predictors were assessed using Mann-Whitney *U* test or Chi-square test. Unsupervised consensus clustering was used to analyze the representativeness and reduce the redundancy of radiomics features. Multivariable logistic regression analysis was performed to build radiomics signature and develop predictive models of EGFR mutation. ROC curve analysis and Delong test were used to compare the predictive performance among individual features and models.

Results: Of the 234 radiomics features, 93 radiomics features with high repeatability and high predictive significance were selected. The radiomics signature, which was built with one histogram and two textural features, showed the best predictive performance (AUC = 0.762 and 0.775 in the training and validation cohort) in comparison with all the clinical characteristics and conventional CT morphological features to differentiate EGFR mutation status ($P < 0.05$). The integrated model was developed with maximum diameter, location, sex and radiomics signature. In the training and validation cohort, the integrated model showed the most optimal predictive performance (AUC = 0.798, 0.818 in the training and validation cohort) compared with the clinical models.

Conclusion: The radiomics signature showed better performance for predicting EGFR mutant than all the clinical and morphological features. Moreover, the integrated model built with radiomics signature, clinical and morphological features outperformed the clinical models, which is helpful for physicians to determine the targeted therapy.

1. Introduction

Lung cancer is the leading cause of cancer-related mortality worldwide [1]. Non-small cell lung cancer (NSCLC) accounts for 85%. With the development of individualized precision therapy, the molecular targeted therapy of NSCLC is becoming more and more popular. The treatment decisions are based on patient's clinic-pathologic characteristics, tumor stage and individual gene mutation status. The most common gene mutation in NSCLC is epidermal growth factor receptor (EGFR) mutation [2,3]. The mutation status determines the

Abbreviations: AIC, Akaike's information criterion; AUC, area under the curve; CEA, carcinoembryonic antigen; CT, computed tomography; DICOM, digital imaging and communications in medicine; EGFR, epidermal growth factor receptor; GGO, ground-glass opacity; GLCM, gray level co-occurrence matrix; GLRLM, gray level run-length matrix; H, histogram; ICC, intra-class correlation coefficient; NCCN, National Comprehensive Cancer Network; NSCLC, non-small cell lung cancer; RLN, run length non-uniformity; ROC, receiver-operating characteristic; TKI, tyrosine kinase inhibitor

* Corresponding authors.
E-mail addresses: czyxfl@smmu.edu.cn (L. Fan), lizhaobin79@163.com (Z. Li).
[1] These authors contributed equally to this work.

https://doi.org/10.1016/j.lungcan.2019.03.025
Received 29 December 2018; Received in revised form 4 March 2019; Accepted 25 March 2019

therapeutic management, in turn affects the prognosis. At present, EGFR tyrosine kinase inhibitors (TKIs), such as erlotinib, gefitinib, and afatinib are recommended as the first-line therapy for NSCLC by the National Comprehensive Cancer Network (NCCN). Patients with EGFR mutations have a higher response rate to EGFR TKIs than those without mutations [4–7]. Therefore, identifying EGFR mutation status is crucial to determine appropriate treatment strategies for NSCLC patients.

The most common approaches for molecular testing are based on biopsies or surgical resection. The two approaches identifying mutation status only rely on a small part of a possibly heterogeneous tumor, which may lead to a false negative result [8]. Recent studies have shown the profound intratumoral genetic heterogeneity in lung cancer [9–11], indicating a significant challenge for the accuracy of molecular profiling by a single biopsy. Both approaches for molecular testing are invasive, and some patients with poor physical conditions are unable to perform biopsies or surgery. Moreover, due to time-consuming procedures, sampling error, and relatively high costs of biopsy, the application in detection of genetic mutation and monitoring therapeutic effect would be limited [12–14]. Therefore, a more reliable, noninvasive and easy method for predicting the gene mutation status is required.

Imaging can reflect intratumoral heterogeneity, and provide longitudinal information on disease state, such as evolution and response to therapy. It has been reported that the EGFR mutation status is correlated with conventional computed tomography (CT) morphological features, such as small lesion size, air bronchogram, pleural retraction, vacuole sign, and presence of ground glass opacity [15,16]. However, the recognition of these CT morphological features depends on the experience of the radiologists. Due to the strong subjectivity and inter- and intra-reader variation, the consistency of each CT morphological feature is not good enough. Radiomics could automatically extract many quantitative features from medical images, containing a large amount of information about tumor phenotypes [17,18]. Radiomics has been used in the prediction of diagnosis, survival, and distant metastasis, as well as gene mutation [19–21]. A few studies [17,22–24] have reported the application of radiomics in predicting EGFR mutation, and most of them mainly focused on clinical data, radiomics features and their comparisons in predictive efficacy. Until now, the studies about the comparison of radiomics signature and CT morphological features, are rare. The aim of this study was first to compare the performance of radiomics signature and CT morphological features in predicting EGFR mutations, then further to develop an optimal predictive model as a more convenient and reliable biomarker for the EGFR mutations of tumor.

2. Materials and methods

2.1. Patient population

A total of 472 consecutive patients with pathologically confirmed lung cancer were recruited retrospectively from April 2012 to October 2016. The inclusion criteria were as follows: (1) pathologically confirmed non-small cell lung cancer by surgery or biopsy; (2) complete EGFR gene mutation test results; (3) available of complete thin-slice chest CT images (≤1 mm) reconstructed in Digital Imaging and Communications in Medicine (DICOM) format before treatment; (4) clinical data integrity. The exclusion criteria were as follows: (1) patients pathologically confirmed as small cell lung cancer (n = 6); (2) no thin-slice chest CT images (n = 51); (3) images with severe artifact (n = 1); (4) tumors accompanying obstructive pneumonia or atelectasis, or with vascular or mediastinal adhesions (n = 10). Then, 404 cases (193 males and 211 females; median age, 61 years; range, 29–81 years) were eligible for the investigation, who were divided into training cohort (243 cases, 113 males and 130 females; median age, 62 years; range, 29–80 years) and validation cohort (161 cases, 80 males and 81 females; median age, 60 years; range, 29–81 years) using computer-generated random numbers (**Supplementary Figure S1**). This retrospective study was approved by our institutional review board, and the need for informed patient consent was waived.

Demographic and clinical data included sex, age, smoking status, serum carcinoembryonic antigen (CEA) level, clinical stage and EGFR mutation status. Tumors were staged pathologically according to the eighth edition of the American Joint Committee on Cancer Staging [25]. EGFR mutations, including mutations of EGFR exons 18–21, were detected using an amplification refractory mutation system with real-time technology.

2.2. Image acquisition and segmentation

The imaging acquisition and segmentation methods used in the study are described in **Supplementary Information 1**. The reproducibility of intra-observer and inter-observer segmentation was confirmed by two experienced thoracic radiologists with 3 years and 13 years of experience. The methods for evaluating repeatability have been validated previously [26].

2.3. Evaluation of CT morphological features

All the thin-slice CT images were interpreted by two thoracic radiologists with 3 years and 13 years of experience who were blinded to each subject's identity and clinical data. CT images were read with mediastinal (width, 300 HU; level, 60 HU) and lung (width, 1500 HU; level, -500 HU) window settings. Decisions on CT morphological features were reached by consensus. A total of 17 CT morphological features were assessed, including maximum diameter, density, location, interface, shape, lobulation, pleural indentation, spiculation, cusp angle, spine-like process, vacuole sign, cavity sign, air bronchograms, vascular convergence, pleura thickening, pleural effusion, and lymphadenopathy. The definitions and scoring rules of morphological features are described in **Supplementary Table S1**.

2.4. Extraction and selection of radiomics features and building of the radiomics signature

In total, 234 radiomics features were extracted from the segmented tumor regions on non-contrast CT images. Features were divided into four groups: (1) shape features, (2) histogram features, (3) gray level co-occurrence matrix (GLCM) features, and (4) gray level run-length matrix (GLRLM) features. The radiomics features were normalized with z-scores. These extractions were performed in MATLAB 2015b (Mathworks, Natick, MA, USA). Detailed descriptions of these features are shown in **Supplementary Information 2**.

Feature selection and radiomics signature building were based on the training cohort. First, inter-/intra-class correlation coefficients (ICCs) were used to evaluate the intra-observer and inter-observer agreement of feature extraction. An ICC > 0.75 is considered as good agreement. Stable and reproducible features were entered in the process of signature building. Second, the association between each feature and the EGFR mutation status was explored using Mann-Whitney *U* test. Features with $p < 0.05$ were reserved. Then, to reduce features' redundancy, we used unsupervised consensus clustering [27] with the partition-around-medoids clustering algorithm and Pearson correlation-based dissimilarity measure, and performed 10,000 bootstraps with 80% item resampling of the candidate features. We varied the cluster number from 2 to 10 and selected the optimal cluster number for unsupervised class discovery on the training cohort. The number of clusters, which gave the highest median cluster consensus across the permuted clustering runs, was selected to produce the stable and unambiguous cluster assignments [28]. For each cluster, we only reserved the most representative medoid feature yielding the highest average consensus index. Finally, we combined the medoid features into a radiomics signature using multivariable logistic regression. The backward step-wise selection with Akaike's information criterion (AIC)

as the stopping rule was applied to implement a further redundancy elimination.

2.5. Development of predictive models and statistical analysis

The statistical analysis was performed using R software (version 3.0.1; R Foundation for Statistical Computing, Vienna, Austria; http://www.Rproject.org). A two-sided P-value < 0.05 was considered statistically significant. Differences in all variables between EGFR wild type and EGFR mutation were assessed using Mann-Whitney *U* test for continuous variables and Fisher's exact test or chi-square test for categorical variables.

In order to develop an optimal model for the prediction of EGFR mutations, three models were built in this study. The first model, including all the clinical and morphological features using multivariable logistic regression, was defined as clinical model 1. The second model, with only the statistically significant clinical characteristics and morphological features using multivariable logistic regression with backward step-wise selection, was defined as clinical model 2. The third model was defined as an integrated model combining statistically significant clinical characteristics, morphological features and radiomics signature in the training cohort by using backward step-wise selection. A nomogram was drawn from the integrated model. ROC curve analysis was used to evaluate the predictive performances of the statistically significant features and models. Then, the Delong test was used to compare the predictive performance between the radiomics signature and other individual features; and between the three models. With the optimal cutoff value obtained from the training cohort, sensitivity, specificity and accuracy were also calculated.

3. Results

3.1. Clinical data and CT morphological features

Among the training cohort, there were 112 patients (46.1%) with EGFR mutation and 131 with EGFR wild type. In the validation cohort, there were 74 (46.0%) patients with EGFR mutation and 87 with EGFR wild type. No significant difference in EGFR mutation rate was found between the training and validation cohort (P > 0.05). (Table 1, Table 2).

In the training cohort, there were significant differences in sex and stage between the EGFR wild type and the EGFR mutant. EGFR mutation rates were significantly higher in women (56.2%) than that in men (34.5%) (P < 0.001); and in stage I-II (50%) than in stage III-IV (32.7%) (P = 0.024). About CT morphological features, maximum diameter (P = 0.012), location (P < 0.001), density (P < 0.001), lymphadenopathy (P = 0.044), vacuole sign (P = 0.041), and air bronchograms (P = 0.013) were statistically different between the two groups. EGFR mutations were found more frequently in peripheral tumors with smaller maximum diameter, GGO, air bronchograms, vacuole sign, and without lymphadenopathy.

3.2. Selection of radiomics features and building of the radiomics signature

After assessing the reproducibility based on the re-segmentation data, 179 features with ICCs > 0.75 were reserved. Meanwhile, Mann-Whitney *U* test indicated that 93 stable features had the potential predictive abilities.

Based on consensus clustering of the selected 93 features, we found the optimal cluster number was four, which induced the highest median cluster consensus of 0.975 in the training cohort, while maximizing consensus within clusters and minimizing the rate of ambiguity in cluster assignments, as shown in Fig. 1. Representing each radiomics phenotype cluster, the four medoid features were X2_histogram (H)_standard_entropy, X0_GLRLM_run length non-uniformity (RLN), X4_H_median and X0_GLCM_homogeneity1, respectively. In the training cohort, there were statistical differences in these medoid features between EGFR wild types and EGFR mutants (P < 0.05) (**Supplementary Table S2**). Multivariable logistic regression analysis showed that three of the medoid features were important predictors; therefore, the calculation formula of radiomics signature score was: score = -0.218 -1.753 × X0_GLRLM_RLN -0.682 × X4_H_median -0.580 × X0_GLCM_homogeneity1. High signature score was associated with high probability of EGFR mutation.

3.3. Development of predictive models and predictive performance

Based on the training cohort, clinical model 1 was derived from all the clinical and morphological features, as shown in **Supplementary Table S3**. Backward step-wise selection was used to build clinical model 2 and showed that sex, density and location were screened into clinical model 2 (**Supplementary Table S4**). The corresponding regression equation of clinical model 2 was as follows: In(P/1-p) = -1.730 + 0.593 × sex + 0.831 × density + 1.006 × location. Integrated model was developed with maximum diameter, location, sex and radiomics signature (**Supplementary Table S5**) and was presented

Table 1
Clinical features of patients in the training and validation cohort.

features	training cohort				validation cohort			
	Total (%)	EGFR- (%)	EGFR+ (%)	*P value*	Total (%)	EGFR- (%)	EGFR+ (%)	*P value*
age[a]	60.7 ± 10.5	60.8 ± 10.7	60.5 ± 10.3	0.657	59.2 ± 10.4	59.7 ± 11.3	58.7 ± 9.2	0.260
sex				< 0.001				0.006
male	113(46.5)	74(65.5)	39(34.5)		80(49.7)	52(65.0)	28(35.0)	
female	130(53.5)	57(43.8)	73(56.2)		81(50.3)	35(43.2)	46(56.8)	
stage				0.024				< 0.001
I-II	188(77.4)	94(50.0)	94(50.0)		138(85.7)	67(48.6)	71(51.4)	
III-IV	55(22.6)	37(67.3)	18(32.7)		23(14.3)	20(87.0)	3(13.0)	
CEA(μg/L)				0.700				0.241
≤5	187(77.0)	102(54.5)	85(45.5)		132(82.0)	68(51.5)	64(48.5)	
5~20	40(16.5)	22(55.0)	18(45.0)		23(14.3)	14(60.9)	9(39.1)	
> 20	16(6.6)	7(43.8)	9(56.2)		6(3.7)	5(83.3)	1(16.7)	
smoking status				0.083				< 0.001
non smoker	178(73.3)	90(50.1)	88(49.9)		112(69.6)	50(44.6)	62(55.4)	
smoker	65(26.7)	41(63.1)	24(36.9)		49(30.4)	37(75.5)	12(24.5)	

Note: The *P* value represents the univariate association between each of clinical features and EGFR mutation. Data are presented as n, or n (%), except where otherwise noted.

Abbreviations: EGFR, epidermal growth factor receptor; CEA, carcinoembryonic antigen.

[a] Mean ± standard deviation.

Table 2
CT morphological features of patients in the training and validation cohort.

features	training cohort				validation cohort			
	Total (%)	EGFR- (%)	EGFR+ (%)	*P value*	Total (%)	EGFR- (%)	EGFR+ (%)	*P value*
maximum diameter[a]	3.12 ± 1.84	3.42 ± 1.98	2.78 ± 1.60	0.012	2.60 ± 1.67	2.81 ± 1.96	2.36 ± 1.21	0.531
location				< 0.001				0.039
central	36(14.8)	29(80.6)	7(19.4)		9(5.6)	8(88.9)	1(11.1)	
peripheral	207(85.2)	102(49.3)	105(50.7)		152(94.4)	79(52.0)	73(48.0)	
shape				0.584				0.090
irregular	76(31.3)	39(51.3)	37(48.7)		44(27.3)	19(43.2)	25(56.8)	
round	167(68.7)	92(55.1)	75(44.9)		117(92.7)	68(58.1)	49(41.9)	
density				< 0.001				0.078
solid	138(56.8)	91(65.9)	47(34.1)		73(45.3)	45(61.6)	28(38.4)	
subsolid	105(43.2)	40(38.1)	65(61.9)		88(54.7)	42(47.7)	46(52.3)	
lymphadenopathy(-)	189(77.8)	95(50.3)	94(49.7)	0.044	139(86.3)	67(48.2)	72(51.8)	< 0.001
lymphadenopathy(+)	54(22.2)	36(66.7)	18(33.3)		22(13.7)	20(90.9)	2(9.1)	
interface				0.659				0.753
ill-defined	7(2.9)	4(57.1)	3(42.9)		2(1.2)	1(50.0)	1(50.0)	
smooth	31(12.8)	19(61.3)	12(38.7)		24(14.9)	15(62.5)	9(37.5)	
coarse	205(84.4)	108(52.7)	97(47.3)		135(83.9)	71(52.6)	64(47.4)	
lobulation(-)	27(11.1)	17(63.0)	10(37.0)	0.317	20(12.4)	13(65.0)	7(35.0)	0.293
lobulation(+)	216(88.9)	114(52.8)	102(47.2)		141(87.6)	74(52.5)	67(47.5)	
spiculation(-)	118(48.6)	62(52.5)	56(47.5)	0.678	97(60.2)	54(55.7)	43(44.3)	0.609
spiculation(+)	125(51.4)	69(55.2)	56(44.8)		64(39.8)	33(51.6)	31(48.4)	
cusp angle(-)	232(95.5)	127(54.7)	105(45.3)	0.232	153(95.0)	82(53.6)	71(46.4)	0.897
cusp angle(+)	11(4.5)	4(36.4)	7(63.6)		8(5.0)	5(62.5)	3(37.5)	
spine-like process(-)	170(70.0)	90(52.9)	80(47.1)	0.644	108(67.1)	63(58.3)	45(41.7)	0.118
spine-like process(+)	73(30.0)	41(56.2)	32(43.8)		53(32.9)	24(45.3)	29(54.7)	
vacuole sign(-)	162(66.7)	95(58.6)	67(41.4)	0.041	81(50.3)	46(56.8)	35(43.2)	0.481
vacuole sign(+)	81(33.3)	36(44.4)	45(55.6)		80(49.7)	41(51.3)	39(48.7)	
cavity sign(-)	219(90.1)	121(55.3)	98(44.7)	0.205	149(92.5)	76(51.0)	73(49.0)	0.007
cavity sign(+)	24(9.9)	10(41.7)	14(58.3)		12(7.5)	11(91.7)	1(8.3)	
air bronchograms				0.013				0.026
none	94(38.7)	46(48.9)	48(51.1)		90(55.9)	49(54.4)	41(45.6)	
natural	35(14.4)	15(42.9)	20(57.1)		22(13.7)	6(27.3)	16(72.7)	
dilated/distorted	17(7.0)	6(35.3)	11(64.7)		4(2.5)	2(50.0)	2(50.0)	
cut-off	97(39.9)	64(66.0)	33(34.0)		45(28.0)	30(66.7)	15(33.3)	
pleural indentation(-)	145(59.7)	85(58.6)	60(41.4)	0.073	98(60.9)	60(61.2)	38(38.8)	0.022
pleural indentation(+)	98(40.3)	46(46.9)	52(53.1)		63(39.1)	27(42.9)	36(57.1)	
thickened pleura(-)	191(78.6)	99(51.8)	92(48.2)	0.213	130(80.7)	68(52.3)	62(47.7)	0.367
thickened pleura(+)	52(21.4)	32(61.5)	20(38.5)		31(19.3)	19(61.3)	12(38.7)	
pleural effusion(-)	222(91.4)	121(54.5)	101(45.5)	0.545	150(93.2)	80(53.3)	70(46.7)	0.508
pleural effusion(+)	21(8.6)	10(47.6)	11(52.4)		11(6.8)	7(63.6)	4(36.4)	
vascular convergence (-)	163(67.1)	87(53.4)	76(46.6)	0.811	108(67.1)	66(61.1)	42(38.9)	0.010
vascular convergence (+)	80(32.9)	44(55.0)	36(45.0)		53(32.9)	21(39.6)	32(60.4)	

Note: The *P* value represents the univariate association between each of CT morphological features and EGFR mutation. Data are presented as n, or n (%), except where otherwise noted.

[a] Mean ± standard deviation.

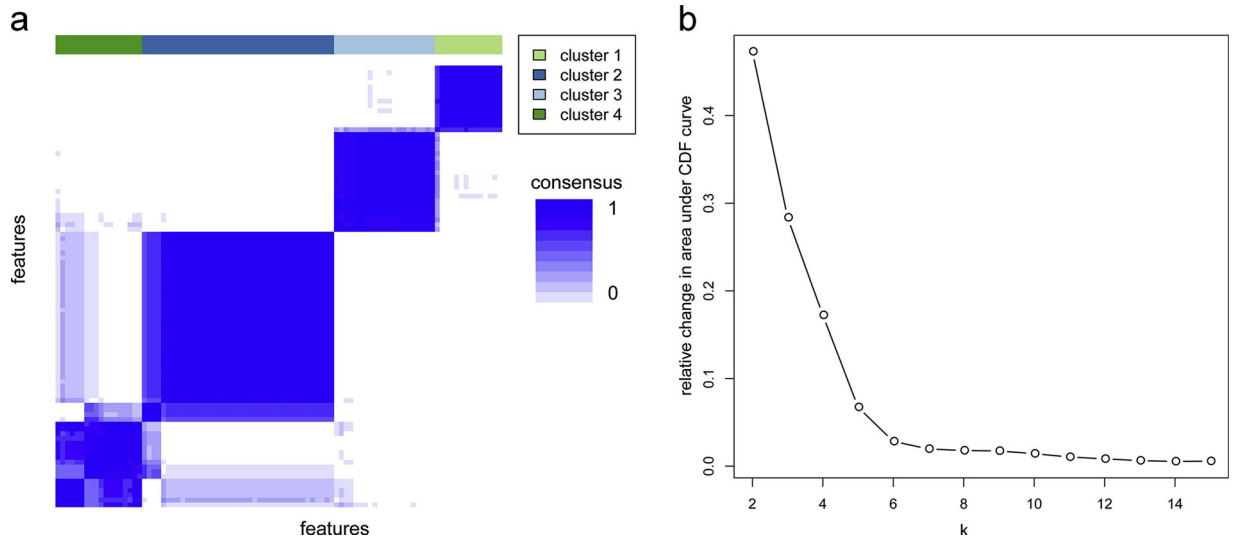

Fig. 1. Results of unsupervised consensus clustering for radiomics features. (a) Consensus heatmap ordered with respect to the obtained clusters. (b) The delta area plot, which depicts the relative consensus increase comparing cluster number k with k+1.

Table 3
Comparisons of predictive performance of statistically significant features and different models.

Characteristic	training cohort					validation cohort				
	AUC	sensitivity	specificity	accuracy	P value	AUC	sensitivity	specificity	accuracy	P value
sex	0.608 (0.547˜0.670)	65.2%	56.5%	60.5%	0.001*	0.610 (0.534˜0.686)	62.2%	59.8%	60.9%	0.002*
stage	0.561 (0.509˜0.613)	83.9%	28.2%	53.9%	< 0.001*	0.595 (0.545˜0.645)	95.9%	23.0%	56.5%	< 0.001*
maximum diameter	0.593 (0.521˜0.665)	45.5%	74.8%	61.3%	< 0.001*	0.529 (0.439˜0.618)	43.2%	54.0%	54.0%	< 0.001*
location	0.579 (0.537˜0.622)	93.8%	22.1%	55.1%	< 0.001*	0.539 (0.506˜0.573)	98.6%	9.2%	50.3%	< 0.001*
density	0.638 (0.577˜0.698)	58.0%	69.4%	64.2%	0.005*	0.569 (0.493˜0.646)	62.2%	51.7%	56.5%	< 0.001*
lymphadenopathy	0.557 (0.506˜0.608)	83.9%	27.4%	53.5%	< 0.001*	0.601 (0.553˜0.650)	97.3%	23.0%	57.1%	< 0.001*
vacuole sign	0.564 (0.504˜0.623)	40.2%	72.5%	57.6%	< 0.001*	0.528 (0.450˜0.606)	52.7%	52.9%	52.8%	< 0.001*
air bronchograms	0.613 (0.546˜0.679)	70.5%	48.9%	58.8%	0.001*	0.613 (0.535˜0.690)	24.3%	90.8%	60.2%	0.003*
radiomics signature	0.762 (0.702˜0.822)	82.1%	61.8%	71.2%	—	0.775 (0.703˜0.847)	87.8%	50.6%	67.7%	—
clinical model 1	0.766 (0.707˜0.824)	75.9%	66.4%	70.8%	0.326#	0.549 (0.459˜0.638)	62.2%	46.0%	53.4%	< 0.001#
clinical model 2	0.693 (0.628˜0.757)	80.4%	53.4%	65.8%	< 0.001#	0.616 (0.532˜0.700)	87.8%	42.5%	63.4%	< 0.001#
integrated model	0.798 (0.742˜0.854)	74.1%	76.3%	75.3%	—	0.818 (0.751˜0.885)	78.4%	73.6%	75.8%	—

Note: Clinical model 1 included all the clinical and morphological features. Clinical model 2 is a simplified clinical model after variable selection by using backward step-wise selection.
*The *P* value represents the difference in AUC between the radiomics signature with other features.
#The *P* value represents the difference in AUC between the integrated model with the clinical models.
—: None.
Abbreviations: ROC, receiver-operating characteristic; AUC, area under the curve.

as a nomogram shown in **Supplementary Figure S2**. The corresponding regression equation of the integrated model was as follows: In (P/1-p) = -2.416 + 1.281 × radiomics signature score + 0.592 × sex + 1.196 × location +0.361 × maximum diameter.

According to ROC curve analysis of the statistically significant features, radiomics signature showed the best performance for discriminating EGFR mutants from EGFR wild types in the training cohort (AUC 0.762, sensitivity 82.1%, specificity 61.8%, accuracy 71.2%, cutoff value -0.403) (Table 3, Fig. 2). In the training cohort, clinical model 1 showed good performance to predict EGFR mutant (AUC 0.766, sensitivity 75.9%, specificity 66.4%, accuracy 70.8%, cutoff value -0.222). And clinical model 2 showed moderate performance (AUC 0.693, sensitivity 80.4%, specificity 53.4%, accuracy 65.8%, cutoff value -0.118). For the integrated model adding radiomics signature, the performance was improved with the increased AUC (0.798), specificity (76.3%), and accuracy (75.3%), and the cutoff value was -0.215.

3.4. Validation of the radiomics signature and models, and comparison of predictive performance

In the validation cohort, radiomics signature had the highest AUC (0.775) to distinguish EGFR wild types from EGFR mutants in comparison with all other individual features (P < 0.05). Clinical model 1 showed poor predictive performance in the validation cohort, indicating that the model was over-fitting due to the inclusion of too many variables. The integrated model was superior to the clinical models, with higher AUC, specificity and accuracy both in the training and validation cohort (Table 3, Fig. 3). Statistically significant difference in AUC was found between the integrated model and clinical model 2 with Delong test (P < 0.001).

4. Discussion

In this study, a radiomics signature composed of three radiomics features was built to differentiate EGFR mutants from EGFR wild types; which showed the best predictive performance in comparison with

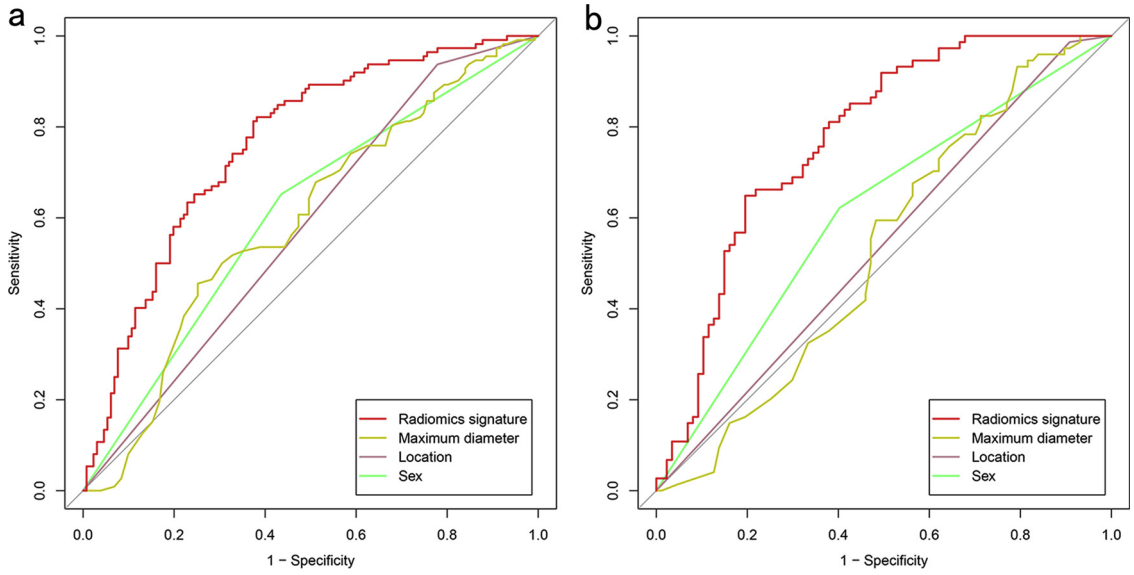

Fig. 2. ROC curves for the independent predictors. Maximum diameter, location, sex and radiomics signature are the independent predictors for EGFR mutant. (a) the training cohort; (b) the validation cohort.

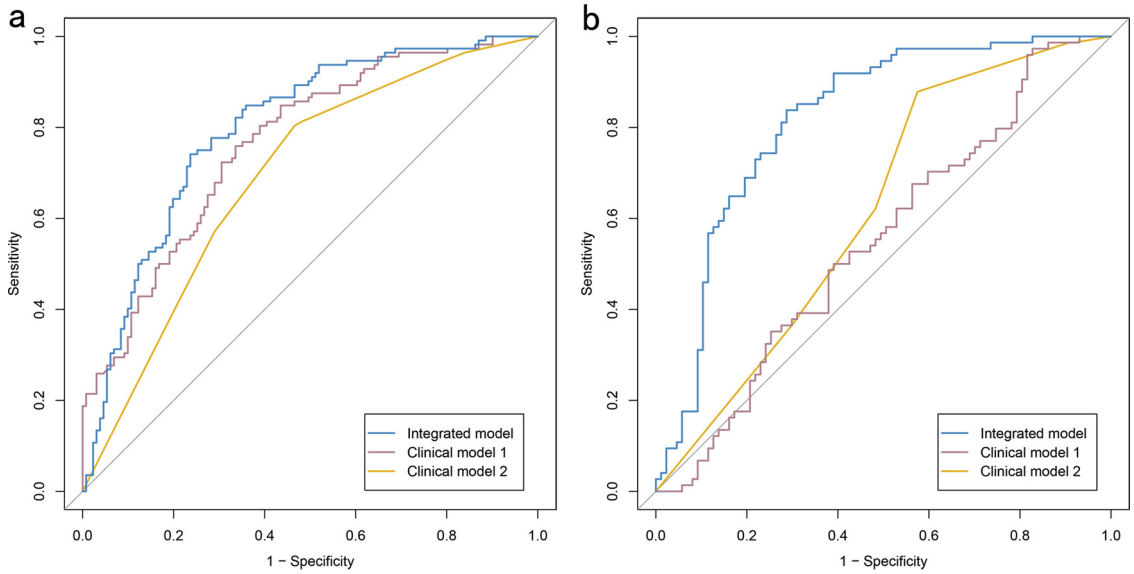

Fig. 3. ROC curves for the clinical models and integrated model. (a) the training cohort; (b) the validation cohort.

clinical characteristics and morphological features. Moreover, the integrated model based on radiomics signature outperformed the clinical models generated with clinical and morphological features. Therefore, the integrated model is a non-invasive and optimal biomarker to detect EGFR mutation status.

The clinical characteristics are the most easily available for NSCLC patients, which are usually expected to be predictors of EGFR mutation. There have been cumulative studies reporting that several clinical factors such as female, non-smoker, adenocarcinoma histology, and East Asian population were associated with EGFR mutation [29,30]. Therefore, in clinical practice, these are the primary considerations for EGFR-TKI treatment. Consistent with most of previous findings, we found EGFR mutation rates were higher in female and never-smoker patients, despite no significant difference in smoking status. Furthermore, the rate of EGFR mutations in early-stage NSCLC patients was significantly higher than that in advanced stage patients, similar to a recent study [22].

In the morphological features of NSCLC lesions, maximum diameter, location, density, lymphadenopathy, vacuole sign, and air bronchograms were associated with EGFR mutation status. Maximum diameter of EGFR mutant group was significantly smaller than that of EGFR wild type. Hence, smaller tumors suggest EGFR mutation, which is consistent with other studies [15,16]. The rate of EGFR mutations in peripheral lung cancer was higher than that in central lung cancer, which may be related to the predominance of adenocarcinoma in peripheral location. Prior studies [30,31] showed EGFR mutation was more common in adenocarcinoma than in squamous cell carcinoma. We also found tumors with GGO were more frequent in the EGFR mutation group than those without GGO, similar to previous studies [16,32]. This may be explained by that adenocarcinomas often manifest as ground glass nodules and have a relatively higher mutation rate of EGFR. Tumors without lymphadenopathy, with vacuole sign and air bronchograms were more likely to be EGFR mutants, which is consistent with previous studies [15,32]. A few other features were also found to be associated with EGFR mutations, such as pleural retraction, absence of emphysema and spiculation [15,29,32]. Morphological features depend on the radiologist's experience and subjective interpretation of the signs, which may explain the low AUCs for the morphological features. Due to over-fitting problem, clinical model 1 is not applicable to other datasets and cannot be recommended in clinical practice. In clinical model 2, sex, density and location were important predictors of EGFR mutations.

In this study, unsupervised consensus clustering was used to reduce the redundancy of features and select representative medoid features to build radiomics signature. Consensus clustering analysis of radiomics features has been used to establish imaging subtypes of cancer, which are associated with specific molecular pathways and prognosis, such as breast cancer [33] and glioblastoma [34]. Two textural features were involved in the radiomics signature, i.e. X0_GLRLM_RLN and X0_GLCM_homogeneity1, which could reflect the heterogeneity of tumors. The numerator of GLRLM_RLN calculates the squared sum of the run-length values of each run-length, while its denominator serves as a normalizing factor. Therefore, the value of GLRLM_RLN tends to emphasize the non-uniform distribution of the run-length. Meanwhile, GLCM_homogeneity1 assumes larger values for smaller gray-level differences in the co-occurrence pairs. Therefore, these features could measure the textural distribution in the ROIs from different aspects, and reflect the heterogeneity of tumors. X0_GLRLM_RLN was the most important feature because of the significant contribution to the radiomics signature (with the highest regression coefficient). We additionally found that GLRLM_RLN was strongly correlated with volume, and the Spearman correlation coefficient reached 0.89, similar to the study by Welch et al. [35]. The volume was also associated with EGFR mutations ($P < 0.05$, AUC = 0.603). On the other hand, considering that maximum diameter was an independent predictor in the integrated model, we believe that tumor size is an effective predictor for EGFR mutation and should pay more attention on this finding in future research and clinical applications. Comparing with the morphological and clinical features, radiomics signature showed the best predictive performance to differentiate EGFR mutation group. Thus, radiomics signature may be served as a surrogate for genetic tests, or as additional information to monitor response to therapy.

Integrating the radiomics signature, the clinical and morphological features, the integrated model was built consisting of maximum diameter, location, sex and radiomics signature. The integrated model showed good performance with higher AUC, better than the radiomics signature and the clinical models in both training and validation cohorts. This finding suggested that the integrated model based on radiomics is more effective to improve the pre-therapy personalized prediction of EGFR mutation. This finding was similar to the previous study by Liu et al. [22], which selected five radiomics features to construct a radiomics model for prediction of EGFR mutation in lung adenocarcinomas. And they found the predictive ability of clinical model increased when combining with radiomics features. Zhang et al. [23] also found the combined model was superior to the model

generated with clinical features alone and the model with radiomics features alone. Although the inclusion criteria, sample size, feature selection approach or modeling methods of previous studies were different from ours, we have also established radiomics-based EGFR prediction models with good predictive performance. Therefore, it is indicated that EGFR mutation status may be indeed related with the imaging phenotypes of tumors, and it is feasible to predict EGFR mutation status by mining intratumoral heterogeneity from medical images. Most of prior studies didn't evaluate morphological characteristics comprehensively. Rios et al. [17] only incorporated two size-based characteristics (maximum diameter and tumor volume) into their radiomics study about predicting EGFR mutation, and found radiomics signature was superior to size-based characteristics. In contrast, we assessed more comprehensive morphological features than those previous studies.

There are some limitations in this study. First, this study is retrospective and single-institution. A prospective multi-institutional study would be performed to improve the generalization ability and optimize the model. It is necessary to develop more efficient model for different datasets and different populations, and to verify our results widely. Second, the radiomics features were derived from the ROIs of manual segmentation. Although the agreement of manual segmentation has been validated, it is time-consuming. Therefore, an automatic segmentation method with high repeatability and accuracy should be developed. If this comes true, the probability of EGFR mutation will be outputted automatically within a few seconds. It holds promise of improving personalized management of the targeted therapy.

5. Conclusion

In conclusion, the radiomics signature would be a better biomarker to predict EGFR mutation status, in comparison with all the clinical and morphological features. Moreover, the integrated model derived from radiomics signature, clinical and morphological features, showed the most optimal predictive performance, which outperformed the clinical models. Therefore, the integrated model may assist physicians to select EGFR-TKI treatment or not.

Funding

This study has received funding by the National Key R&D Program of China [grant number 2016YFE0103000, 2017YFC1308703], the National Natural Science Foundation of China [grant Number 81871321, 81370035], the Youth Fund of the National Natural Science Foundation of China [grant number 81501618, 81501470]. The funders have no role in the study design, data collection, data analysis and writing the manuscripts.

Conflict of interest

None to declare.

Acknowledgements

The authors would like to thank Prof. Jie Tian's team (CAS Key Laboratory of Molecular Imaging, Institute of Automation, Chinese Academy of Sciences) for their help with statistical advice and statistical analysis.

Appendix A. Supplementary data

Supplementary material related to this article can be found, in the online version, at doi:https://doi.org/10.1016/j.lungcan.2019.03.025.

References

[1] R.L. Siegel, K.D. Miller, A. Jemal, Cancer statistics, 2018, CA Cancer J. Clin. 68 (1) (2018) 7–30, https://doi.org/10.3322/caac.21442.
[2] Y. Jia, C.H. Yun, E. Park, et al., Overcoming EGFR T790M and C797S resistance with mutant-selective allosteric inhibitors, Nature 534 (7605) (2016) 129–132, https://doi.org/10.1038/nature17960.
[3] J.F. Gainor, A.M. Varghese, S.H. Ou, et al., ALK rearrangements are mutually exclusive with mutations in EGFR or KRAS: an analysis of 1,683 patients with non–small cell lung cancer, Clin. Cancer Res. 19 (15) (2013) 4273–4281, https://doi.org/10.1158/1078-0432.CCR-13-0318.
[4] H. Sasaki, K. Endo, K. Okuda, et al., Epidermal growth factor receptor gene amplification and gefitinib sensitivity in patients with recurrent lung cancer, J. Cancer Res. Clin. Oncol. 134 (5) (2008) 569–577, https://doi.org/10.1007/s00432-007-0320-z.
[5] G.J. Riely, W. Pao, D. Pham, et al., Clinical course of patients with non-small cell lung cancer and epidermal growth factor receptor exon 19 and exon 21 mutations treated with gefitinib or erlotinib, Clin. Cancer Res. 12 (3 Pt 1) (2006) 839–844, https://doi.org/10.1158/1078-0432.CCR-05-1846.
[6] N. Thatcher, A. Chang, P. Parikh, et al., Gefitinib plus best supportive care in previously treated patients with refractory advanced non-small-cell lung cancer: results from a randomised, placebo-controlled, multicentre study (Iressa Survival Evaluation in Lung Cancer), Lancet 366 (9496) (2005) 1527–1537, https://doi.org/10.1016/S0140-6736(05)67625-8.
[7] T. Stinchcombe, M. Socinski, Gefitinib in advanced non-small cell lung cancer: does it deserve a second chance? Oncologist 13 (9) (2008) 933–944, https://doi.org/10.1634/theoncologist.2008-0019.
[8] K. Taniguchi, J. Okami, K. Kodama, et al., Intratumor heterogeneity of epidermal growth factor receptor mutations in lung cancer and its correlation to the response to gefitinib, Cancer Sci. 99 (5) (2008) 929–935, https://doi.org/10.1111/j.1349-7006.2008.00782.x.
[9] H. Bai, Z. Wang, Y. Wang, et al., Detection and clinical significance of intratumoral EGFR mutational heterogeneity in chinese patients with advanced non-small cell lung cancer, PLoS One 8 (2) (2013) e54170, , https://doi.org/10.1371/journal.pone.0054170.
[10] J. Song, D. Dong, Y. Huang, et al., Association between tumor heterogeneity and progression-free survival in non-small cell lung cancer patients with EGFR mutations undergoing tyrosine kinase inhibitors therapy, Conf. Proc. IEEE Eng. Med. Biol. Soc. (2016) 1268–1271, https://doi.org/10.1109/EMBC.2016.7590937.
[11] N. Tomonaga, Y. Nakamura, H. Yamaguchi, et al., Analysis of intratumor heterogeneity of EGFR mutations in mixed type lung adenocarcinoma, Clin. Lung Cancer 14 (5) (2013) 521–526, https://doi.org/10.1016/j.cllc.2013.04.005.
[12] N.I. Lindeman, P.T. Cagle, M.B. Beasley, et al., Molecular testing guideline for selection of lung cancer patients for EGFR and ALK tyrosine kinase inhibitors: guideline from the College of American Pathologists, International Association for the Study of Lung Cancer, and Association for Molecular Pathology, J. Mol. Diagn. 15 (4) (2013) 415–453, https://doi.org/10.1016/j.jmoldx.2013.03.001.
[13] M. Gerlinger, A.J. Rowan, S. Horswell, et al., Intratumor heterogeneity and branched evolution revealed by multiregion sequencing, N. Engl. J. Med. 366 (10) (2012) 883–892, https://doi.org/10.1056/NEJMoa1113205.
[14] P.L. Bedard, A.R. Hansen, M.J. Ratain, et al., Tumour heterogeneity in the clinic, Nature 501 (7467) (2013) 355–364, https://doi.org/10.1038/nature12627.
[15] S. Rizzo, F. Petrella, V. Buscarino, et al., CT Radiogenomic Characterization of EGFR, K-RAS, and ALK Mutations in Non-Small Cell Lung Cancer, Eur. Radiol. 26 (1) (2016) 32–42, https://doi.org/10.1007/s00330-015-3814-0.
[16] J.S. Hsu, M.S. Huang, C.Y. Chen, et al., Correlation between EGFR mutation status and computed tomography features in patients with advanced pulmonary adenocarcinoma, J. Thorac. Imaging 29 (6) (2014) 357–363, https://doi.org/10.1097/RTI.0000000000000116.
[17] V.E. Rios, C. Parmar, Y. Liu, et al., Somatic mutations drive distinct imaging phenotypes in lung cancer, Cancer Res. 77 (14) (2017) 3922–3930, https://doi.org/10.1158/0008-5472.CAN-17-0122.
[18] R.J. Gillies, P.E. Kinahan, H. Hricak, Radiomics: images are more than pictures, they are data, Radiology 278 (2) (2016) 563–577, https://doi.org/10.1148/radiol.2015151169.
[19] H.J. Aerts, E.R. Velazquez, R.T. Leijenaar, et al., Decoding tumour phenotype by noninvasive imaging using a quantitative radiomics approach, Nat. Commun. 5 (2014) 4006, https://doi.org/10.1038/ncomms5006.
[20] S. Hawkins, H. Wang, Y. Liu, et al., Predicting malignant nodules from screening CT scans, J. Thorac. Oncol. 11 (12) (2016) 2045–2047, https://doi.org/10.1016/j.jtho.2016.07.002.
[21] T.P. Coroller, P. Grossmann, Y. Hou, et al., CT-based radiomic signature predicts distant metastasis in lung adenocarcinoma, Radiother. Oncol. 114 (3) (2015) 345–350, https://doi.org/10.1016/j.radonc.2015.02.015.
[22] Y. Liu, J. Kim, Y. Balagurunathan, et al., Radiomic features are associated with EGFR mutation status in lung adenocarcinomas, Clin. Lung Cancer 17 (5) (2016) 441–448, https://doi.org/10.1016/j.cllc.2016.02.001 e6.
[23] L. Zhang, B. Chen, X. Liu, et al., Quantitative biomarkers for prediction of epidermal growth factor receptor mutation in non-small cell lung cancer, Transl. Oncol. 11 (1) (2017) 94–101, https://doi.org/10.1016/j.tranon.2017.10.012.
[24] S.S. Yip, J. Kim, T.P. Coroller, et al., Associations between somatic mutations and metabolic imaging phenotypes in non–small cell lung cancer, J. Nucl. Med. 58 (4) (2016) 569–576, https://doi.org/10.2967/jnumed.116.181826.
[25] W.D. Travis, H. Asamura, A.A. Bankier, et al., The IASLC lung cancer staging project: proposals for coding T categories for subsolid nodules and assessment of tumor

size in part-solid tumors in the forthcoming eighth edition of the TNM classification of lung cancer, J. Thorac. Oncol. 11 (8) (2016) 1204–1223, https://doi.org/10.1016/j.jtho.2016.03.025.
[26] L. Fan, M.J. Fang, Z.B. Li, et al., Radiomics signature: a biomarker for the preoperative discrimination of lung invasive adenocarcinoma manifesting as a ground-glass nodule, Eur. Radiol. (2018) 1–9, https://doi.org/10.1007/s00330-018-5530-z.
[27] M.D. Wilkerson, D.N. Hayes, ConsensusClusterPlus: a class discovery tool with confidence assessments and item tracking, Bioinformatics 26 (12) (2010) 1572–1573, https://doi.org/10.1093/bioinformatics/btq170.
[28] S. Monti, P. Tamayo, J. Mesirov, et al., Consensus Clustering: a resampling-based method for class discovery and visualization of gene expression microarray data, Mach. Learn. 52 (1-2) (2003) 91–118, https://doi.org/10.1023/A:1023949509487.
[29] J.Y. Zhou, J. Zheng, Z.F. Yu, et al., Comparative analysis of clinicoradiologic characteristics of lung adenocarcinomas with ALK rearrangements or EGFR mutations, Eur. Radiol. 25 (5) (2015) 1257–1266, https://doi.org/10.1007/s00330-014-3516-z.
[30] M. Locatelli-Sanchez, S. Couraud, D. Arpin, et al., Routine EGFR molecular analysis in non-small-cell lung cancer patients is feasible: exons 18–21 sequencing results of 753 patients and subsequent clinical outcomes, Lung 191 (5) (2013) 491–499, https://doi.org/10.1007/s00408-013-9482-4.
[31] Y. Lee, H.J. Lee, Y.T. Kim, et al., Imaging characteristics of stage I non-small cell lung cancer on CT and FDG-PET: relationship with epidermal growth factor receptor protein expression status and survival, Korean J. Radiol. 14 (2) (2013) 375–383, https://doi.org/10.3348/kjr.2013.14.2.375.
[32] Y. Liu, J. Kim, F. Qu, et al., CT Features associated with epidermal growth factor receptor mutation status in patients with lung adenocarcinoma, Radiology 280 (1) (2016) 271–280, https://doi.org/10.1148/radiol.2016151455.
[33] J. Wu, Y. Cui, X. Sun, et al., Unsupervised clustering of quantitative image phenotypes reveals breast cancer subtypes with distinct prognoses and molecular pathways, Clin. Cancer Res. 23 (13) (2017) 3334–3342, https://doi.org/10.1158/1078-0432.CCR-16-2415.
[34] H. Itakura, A.S. Achrol, L.A. Mitchell, et al., Magnetic resonance image features identify glioblastoma phenotypic subtypes with distinct molecular pathway activities, Sci. Transl. Med. 7 (303) (2015) 303ra138, https://doi.org/10.1126/scitranslmed.aaa7582.
[35] M.L. Welch, C. Mcintosh, B. Haibe-Kains, et al., Vulnerabilities of radiomic signature development: The need for safeguards, Radiother. Oncol. 130 (2019) 2–9, https://doi.org/10.1016/j.radonc.2018.10.027.